V. DYNAMIC TRANSPORT STUDIES

A. CRUSHED-ROCK COLUMNS

Generally, batch-sorption experiments, which were discussed in the previous chapter, are used to identify sorption mechanisms and to obtain sorption distribution coefficients (Triay et al. 1996a, 1996b). Such experiments are fast, easy, and inexpensive compared to other types of sorption experiments. In this section, we discuss our attempts to verify the results of earlier batch-sorption measurements by performing crushed-tuff column studies under flowing conditions without significantly changing the surface properties of the tuff. By comparing differences with the batch-sorption measurements, such studies would be most sensitive to multiple-species formation, colloid formation, and any other geochemical reactions (such as changes in surface reactivity due to agitation) not adequately described by batch-sorption distribution coefficients. In these crushed-tuff column experiments, we investigated mass-transfer kinetics by studying radionuclide migration as a function of water velocity.

Column elution curves can be characterized by two parameters: the time of arrival of the radionuclide eluted through the column and the broadness (dispersion) of the curve. The arrival time depends on the retardation factor, R_f, which, for soluble radionuclides, depends, in turn, on the sorption distribution coefficient, K_d. Significant deviations (those larger than expected based on sampling variability) in arrival time from that predicted on the basis of the batch-sorption distribution coefficients indicate one of the following problems:

- the presence of more than one chemical species that are not readily exchanged and that have different selectivities in tuff minerals,
- the presence of the radionuclide as a colloid,
- extremely slow sorption kinetics,
- nonreversibility of the sorption process, and
- solubility effects due to the presence of solids.

The broadness, or apparent dispersion, of the curve depends on

- the kinetics and reversibility of sorption and
- the linearity of the isotherm that describes the dependence of sorption on radionuclide concentration.

The main goal of our study was to test the necessary assumptions made in using values of the sorption distribution coefficient, K_d, (determined by batch-sorption measurements) to describe hydrologic transport. These assumptions are:

1. microscopic equilibrium is attained between the solution species and the adsorbate,
2. only one soluble chemical species is present (or if more than one is present, they interchange rapidly),
3. the radionuclides in the solid phase are adsorbed on mineral surfaces (that is, they are not precipitated), and
4. the dependence of sorption on concentration is described by a linear isotherm.

The importance of verifying these assumptions can be demonstrated by the following hypothetical cases. If equilibrium were not attained in the batch experiments (violation of assumption 1), the retardation of radionuclides could be dependent on groundwater velocity. If a radionuclide were present in solution as an anionic and a cationic species and solution equilibrium were not maintained (violation of assumption 2), the batch measurement would predict a single retardation factor, whereas in a flowing system, the anion could move unimpeded (its size and charge excluding it from the pores of the Yucca Mountain tuff) compared to movement of the cation. If the radionuclide had precipitated in the batch experiments (violation of assumption 3), the value of the K_d thus determined would be meaningless, and depending on the precipitation mechanism, colloid transport could be important. If the isotherm was nonlinear (violation of assumption 4), the migration front of the radionuclides in a column study would usually broaden, appearing as increased dispersion over that observed for nonsorbing tracers.

Experimental Procedures

Groundwaters and solutions

Because the J-13 and UE-25 p#1 well waters that bound the Yucca Mountain groundwaters are both oxidizing (Ogard and Kerrisk 1984), all the batch-sorption and column experiments were performed under oxidizing conditions. In the batch-sorption experiments, both groundwaters (filtered by a 0.05-μm filter) were used, but in the column experiments, we used J-13 water (filtered) and a sodium-bicarbonate buffer that simulated UE-25 p#1 groundwater (because of the unavailability of water from this well). The synthetic UE-25 p#1 water was prepared by dissolving 0.39 g of Na_2CO_3 and 8.90 g of $NaHCO_3$ in 10 liters of deionized water, which duplicates the larger amount of bicarbonate in reference, or on-site, UE-25 p#1 water.

In the column experiments, we used neptunium and plutonium solutions prepared in the same way as for the batch-sorption experiments—by taking an aliquot of a well-characterized $^{237}Np(V)$ or $^{239}Pu(V)$ acidic stock and diluting it in the water being studied. We also used tritium and pertechnetate solutions, which were similarly prepared by adding an aliquot of ^{3}H or ^{95m}Tc acidic stock to the groundwater being studied.

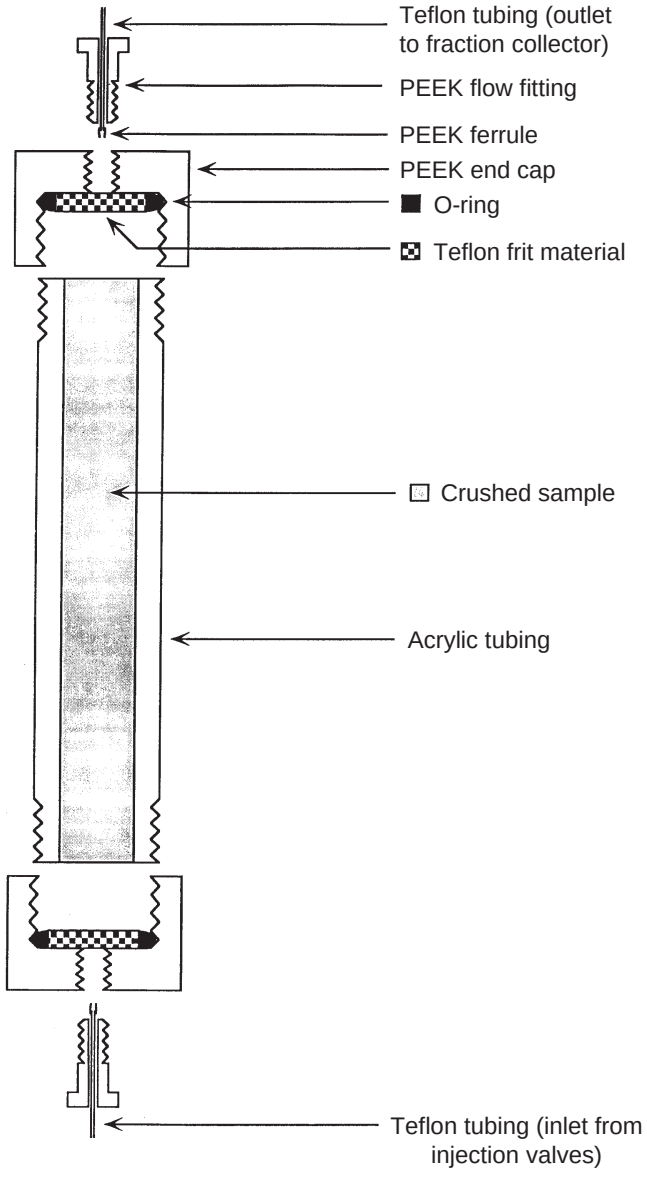

Figure 96. Cross Section of Crushed-rock Columns.

Crushed-rock column procedure

The details of the crushed-rock column experimental setup and procedure are illustrated in Figs. 96 and 97. We packed plexiglas columns with crushed tuff by using a continuously agitated wet slurry, a technique that provides a relatively homogeneous packing nearly free of stratification. As in the batch-sorption experiments, all tuff samples had previously been crushed and wet-sieved (with the groundwater being used in the experiment) to obtain particle sizes ranging from 75 to 500 μm.

After establishing the desired flow rate in the tuff column using the desired groundwater, we injected an aliquot of the radionuclide solution and then used a syringe pump to elute the radionuclide through the column. The breakthrough or elution curve was measured. Tritiated water was used to measure the free volume of the column, which excludes dead-end pore volume. The concentration of tritium, pertechnetate, ^{239}Pu, or ^{237}Np in the eluent was measured by liquid-scintillation counting. The crushed-rock column dimensions and

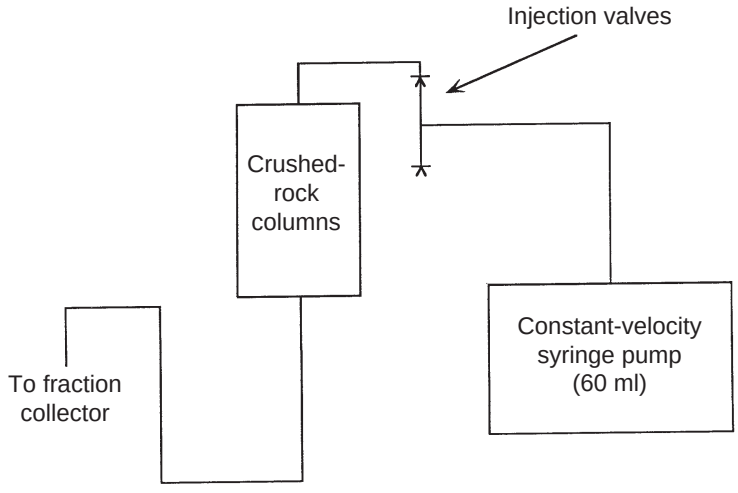

Figure 97. Flow Chart of Crushed-rock Column Experiment.

flow velocities that we used followed the guidelines provided by Relyea (1982).

Relationship between column and batch experiments

We measured the batch-sorption distribution coefficients under static conditions by equilibrating a solution containing the radionuclides with a sample of crushed tuff. If we assume that equilibrium is achieved between a single aqueous chemical species and the species adsorbed on the solid phase, the rate at which a radionuclide moves through a column can simply be related to the sorption distribution coefficient, K_d. The relationship between the retardation factor, R_f, obtained from column-transport experiments, and the values of K_d, obtained from batch-sorption experiments, is generally given by

$$R_f = 1 + \frac{\rho_b}{\epsilon} K_d \ , \qquad (40)$$

where ρ_b is the dry bulk density (including pores) and ϵ is the porosity of the column. Hiester and Vermeulen (1952) derived this equation and carefully described its underlying assumptions.

To test these assumptions, the radionuclide solution used in the batch-sorption measurements was eluted through columns containing tuff samples that came from the same drill hole and depth interval and that had been crushed and sieved to the same size fraction as samples used in the batch-sorption studies.

Results and Discussion

The most comprehensive explanation of the fate of reactive and nonreactive solutes and suspended particles in porous and fractured media has been presented by de Marsily (1986, Chapter 10). The transport of radionuclides in porous media is governed by advection, diffusion, or kinematic dispersion. Advection is the mechanism in which dissolved species are carried along by the movement of fluid. Diffusion causes species to be transferred from zones of high concentration to zones of low concentration. Kinematic dispersion is a mixing phenomenon linked to the heterogeneity of the microscopic velocities inside the porous medium. The migration of a solute in a saturated porous medium is described by the following transport equation

$$\nabla \cdot (\mathbf{D}\,\nabla C - C\mathbf{U}) = \epsilon \frac{\partial C}{\partial t} + Q \ , \qquad (41)$$

where **D** is the dispersion tensor, C is the concentration of solute in the solution phase, **U** is the filtration velocity (Darcy's velocity), ϵ is the porosity, t is time, and Q is a "net source or sink term" that accounts for such things as reactivity or adsorption.

For the case of a sorbing, nonreactive solute, the equation becomes

$$\nabla \cdot (\mathbf{D}\,\nabla C - C\mathbf{U}) = \epsilon \frac{\partial C}{\partial t} + \rho_b \frac{\partial F}{\partial t} \ , \qquad (42)$$

where ρ_b, again, is the dry bulk density of the medium and F is the mass of solute sorbed per unit mass of solid.

Dispersion has three components: the longitudinal

dispersion coefficient in the direction of the flow, D_L, and the transverse dispersion coefficient, D_T, in the two directions at right angles to the velocity of the flow. These components are given by

$$D_L = \epsilon d + \alpha_L |U| \text{ and}$$
$$D_T = \epsilon d + \alpha_T |U| \quad , \tag{43}$$

where d is the effective diffusion coefficient in the medium and α is dispersivity.

The characteristics of the sorption determine the actual relationship between F and C. For the case in which sorption is linear, reversible, and instantaneous, the ratio between F and C is simply equal to the sorption distribution coefficient:

$$\frac{F}{C} = K_d \ . \tag{44}$$

Substitution of Eqn. 44 into Eqn. 42 yields

$$\nabla \cdot (\mathbf{D}\,\nabla C - C\mathbf{U}) = \epsilon\left[1 + \frac{\rho_b}{\epsilon} K_d\right]\frac{\partial C}{\partial t} \ . \tag{45}$$

The expression in brackets in Eqn. 45 corresponds to the retardation factor, R_f, given earlier (Eqn. 40). Thus, we have a way to compare sorption coefficients obtained under advective, diffusive, and dispersive conditions with sorption coefficients obtained from batch-sorption experiments. However, this approach is valid only if sorption is linear, reversible, and instantaneous.

Neptunium results

We measured the elution of Np(V) as a function of water velocity through zeolitic, devitrified, and vitric crushed tuff in columns with J-13 well water and with synthetic UE-25 p#1 water. The elution curves have been previously published (Triay et al. 1996c). We calculated the porosity as the free column volume divided by the total column volume (free volume was defined as the volume of tritium solution that had to be eluted to recover 50% of the injected tritium). We then calculated values of R_f for the column experiments by dividing the free column volume into the volume of neptunium solution that had to be eluted to recover 50% of the injected ^{237}Np. From these values of R_f, we used Eqn. 40 to calculate the column sorption-distribution coefficients listed in Table 27.

How do the earlier results of batch-sorption experiments (Triay et al.1996a, 1996b) compare with the results of the crushed-tuff column experiments? Inspection of Table 27 indicates good agreement between the values of K_d obtained by the two approaches, which means that the arrival time of ^{237}Np can be predicted from a value for K_d. On the other hand, the broad, dispersive shape of the elution curves indicates that sorption of neptunium onto zeolitic and vitric tuffs appears to be nonlinear, nonreversible, or noninstantaneous. Previous work has found that sorption of neptunium onto clinoptilolite-rich tuffs is rapid (Triay et al. 1996a) and can be fit with a linear isotherm (Triay et al. 1996b). Consequently, the degree of reversibility of neptunium sorption onto zeolitic and vitric tuffs may be the most likely reason for the apparent dispersivity in the tuff-column elution curves.

The elution curves also reveal that, regardless of the water being studied, the elution of ^{237}Np does not precede the elution of tritium for any of the tuffs. This observation is extremely important because if charge-exclusion effects were to cause the neptunyl-carbonato complex (an anion) to elute faster than neutral tritiated water molecules, significant neptunium releases could occur at Yucca Mountain. Another important observation that can be drawn from these experiments is that values of K_d can be used to obtain accurate or conservative estimates for the performance-assessment calculations of neptunium transport through Yucca Mountain tuffs.

Neptunium summary

- Using crushed-rock columns, we studied the retardation of ^{237}Np by zeolitic, devitrified, and vitric tuffs in sodium-bicarbonate waters under oxidizing conditions (at room temperature, under atmospheric conditions, and using different water velocities).

- We compared the sorption distribution coeffi-

Table 27. Comparison of Neptunium K_d Values from Batch and Column Measurements

Column Number	Tuff Sample	Water Type	Batch K_d (ml/g)	Column K_d (ml/g)
1	G4-1508, zeolitic	J-13	1.7 ± 0.4 (G4-1510)	1.7
2	G4-1508, zeolitic	J-13	1.7 ± 0.4 (G4-1510)	1.2
3	G4-1505, zeolitic	J-13	2.1 ± 0.4	2.8
4	G4-1505, zeolitic	Syn. UE-25 p#1	0.2 ± 0.3 (G4-1506)	0.4
5	G4-1505, zeolitic	Syn. UE-25 p#1	0.2 ± 0.3 (G4-1506)	0.2
6	G4-1505, zeolitic	Syn. UE-25 p#1	0.2 ± 0.3 (G4-1506)	0.2
7	G4-268, devitrified	J-13	–0.04 ± 0.2	0.07
8	G4-268, devitrified	J-13	–0.04 ± 0.2	0.01
9	G4-268, devitrified	J-13	–0.04 ± 0.2	0.02
10	G4-268, devitrified	J-13	–0.04 ± 0.2	0.01
11	G4-272, devitrified	Syn. UE-25 p#1	0.2 ± 0.3 (G4-270)	0.06
12	G4-268, devitrified	Syn. UE-25 p#1	0.2 ± 0.3 (G4-270)	0.03
13	G4-268, devitrified	Syn. UE-25 p#1	0.2 ± 0.3 (G4-270)	0.03
14	GU3-1407, vitric	J-13	0.1 ± 0.5	0.2
15	GU3-1407, vitric	J-13	0.1 ± 0.5	0.1
16	GU3-1405, vitric	J-13	0.03 ± 0.2	0.1
17	GU3-1405, vitric	Syn. UE-25 p#1	0.2 ± 0.4 (GU3-1407)	0.1
18	GU3-1405, vitric	Syn. UE-25 p#1	0.2 ± 0.4 (GU3-1407)	0.1
19	GU3-1405, vitric	Syn. UE-25 p#1	0.2 ± 0.4 (GU3-1407)	0.1

cients obtained from the column experiments under flowing conditions to those obtained from batch-sorption experiments under static conditions.

- The column and batch distribution coefficients agreed well for all tuffs regardless of the groundwater studied and the water velocity used for the column experiments.

- We found that batch-sorption distribution coefficients predict well the arrival time for neptunium eluted through a crushed-rock column.

- The apparent dispersivity of the neptunium elution curves through the zeolitic and vitric tuffs indicates that the sorption is either nonlinear, irreversible, or noninstantaneous, which means the transport cannot be completely described using a sorption distribution coefficient. The reversibility of neptunium sorption onto tuff will be studied as the most likely reason for the apparent dispersivity of the elution curves.

- The use of a batch-sorption distribution coefficient to calculate neptunium transport through Yucca Mountain tuffs would result in conservative values for neptunium release.

- Neptunium never eluted prior to the nonsorbing radionuclide (tritiated water) used in the column experiments. Thus, charge exclusion does not appear to exclude neptunium from the tuff pores.

- The general trends previously observed for neptunium sorption using batch-sorption experiments were corroborated by these column experiments:

a) neptunium sorption onto devitrified and vitric tuffs is minimal; and
b) neptunium sorption onto zeolitic tuffs decreases as the amount of sodium and bicarbonate/carbonate in the groundwaters increases.

Plutonium and technetium results

The elution of Pu(V) through zeolitic, devitrified, and vitric crushed tuff was measured in columns with J-13 well water and with synthetic UE-25 p#1 water. The elution curves for these experiments (Figs. 98 through 107) indicate that vitric and zeolitic tuffs sorb plutonium significantly, which is probably due to their clay content. The shape of the elution curves for plutonium indicates that use of K_d values to predict plutonium transport through Yucca Mountain tuffs will predict plutonium releases conservatively. Results by Triay et al. (1995a) indicate that plutonium sorption onto tuffs is a slow process and probably due to a redox reaction occurring at the tuff surfaces. To verify these batch-sorption results, which suggest that plutonium sorption, even to the lowest sorbing tuff type (devitrified), could be significant, the migration of plutonium as a function of flow velocity was measured in devitrified tuff using J-13 and UE-25 p#1 waters. Inspection of these elution curves (Figs. 108 and 109) confirms the trends observed using batch-sorption techniques; the elution curves observed for these columns are consistent with slow sorption kinetics.

The elution of pertechnetate was also studied in devitrified, vitric, and zeolitic tuffs in J-13 and synthetic UE-25 p#1 waters as a function of flow velocity. Inspection of the elution curves (Figs. 110 through 115) indicate that anion-exclusion effects for pertechnetate in crushed tuff are essentially negligible except in the case of technetium transport through zeolitic tuff in J-13 well water (Fig. 114). In this case, the anion-exclusion effect is small but measurable.

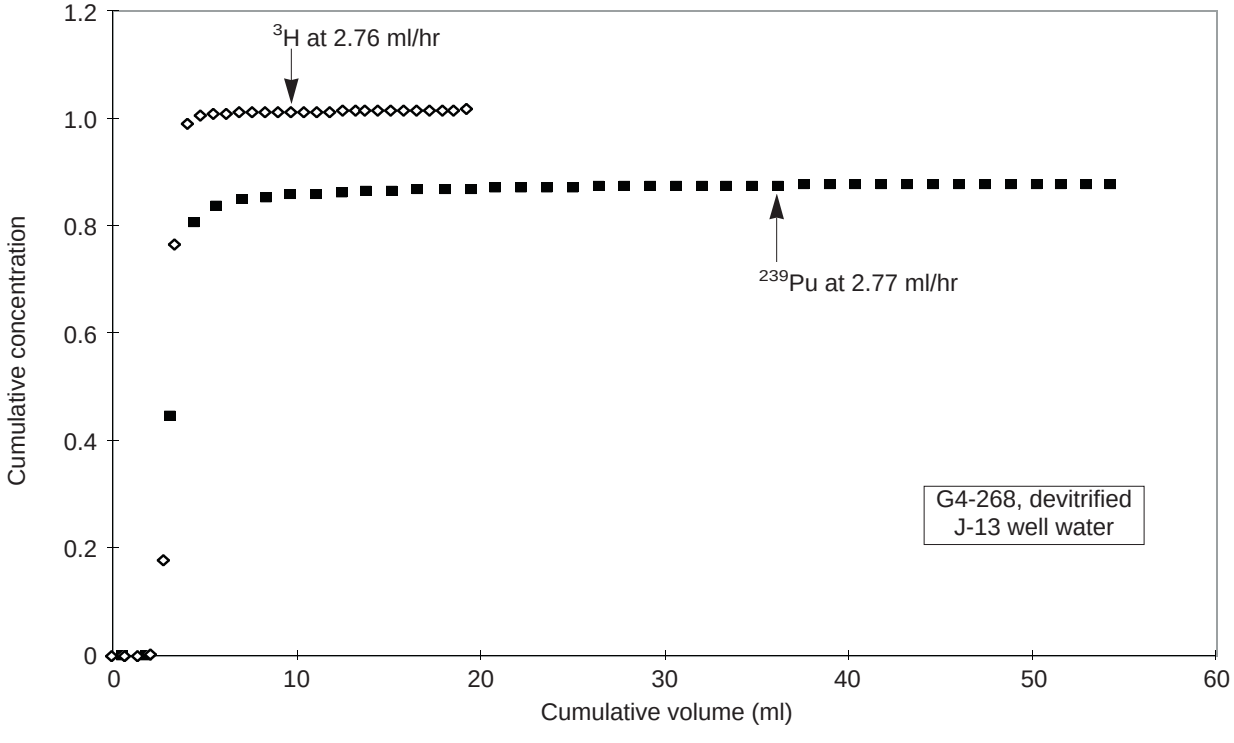

Figure 98. Column 1: Plutonium through Devitrified Tuff. This plot shows the elution curves for tritium and plutonium-239 through devitrified tuff sample G4-268 with J-13 well water.

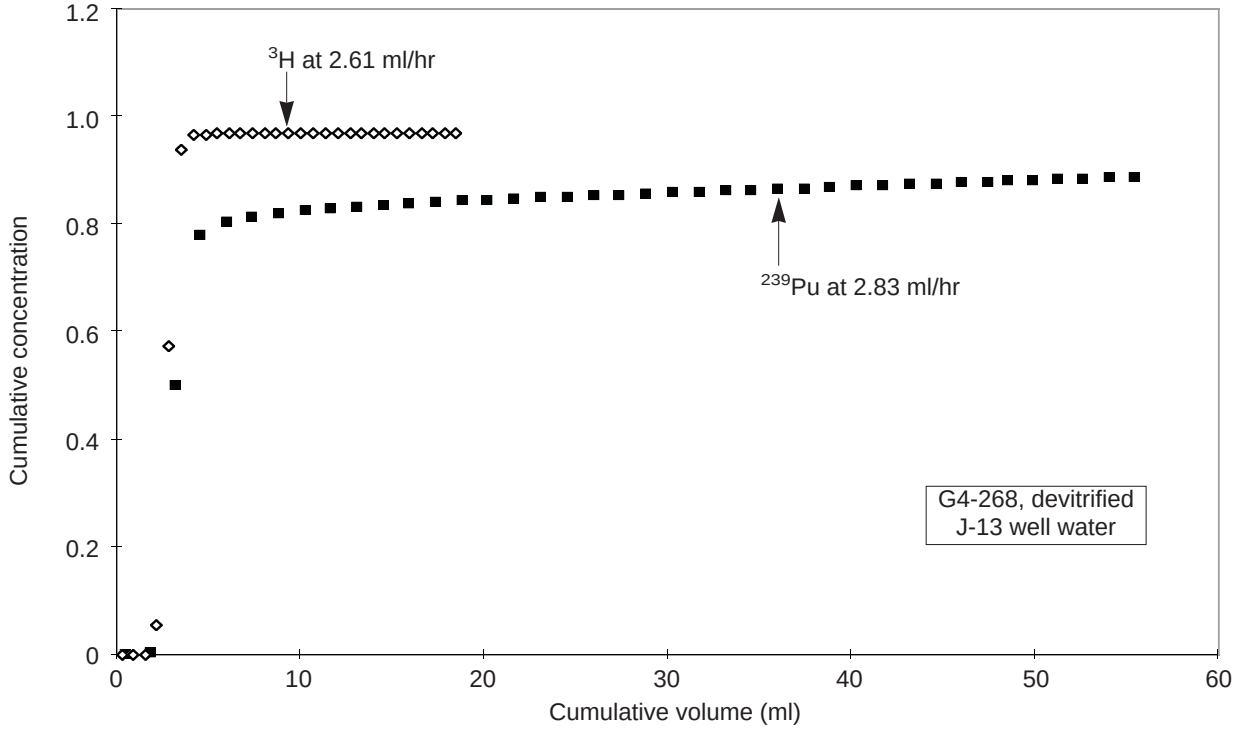

Figure 99. Column 2: Plutonium through Devitrified Tuff. This plot shows a second set of elution curves for tritium and plutonium-239 through devitrified tuff sample G4-268 with J-13 well water.

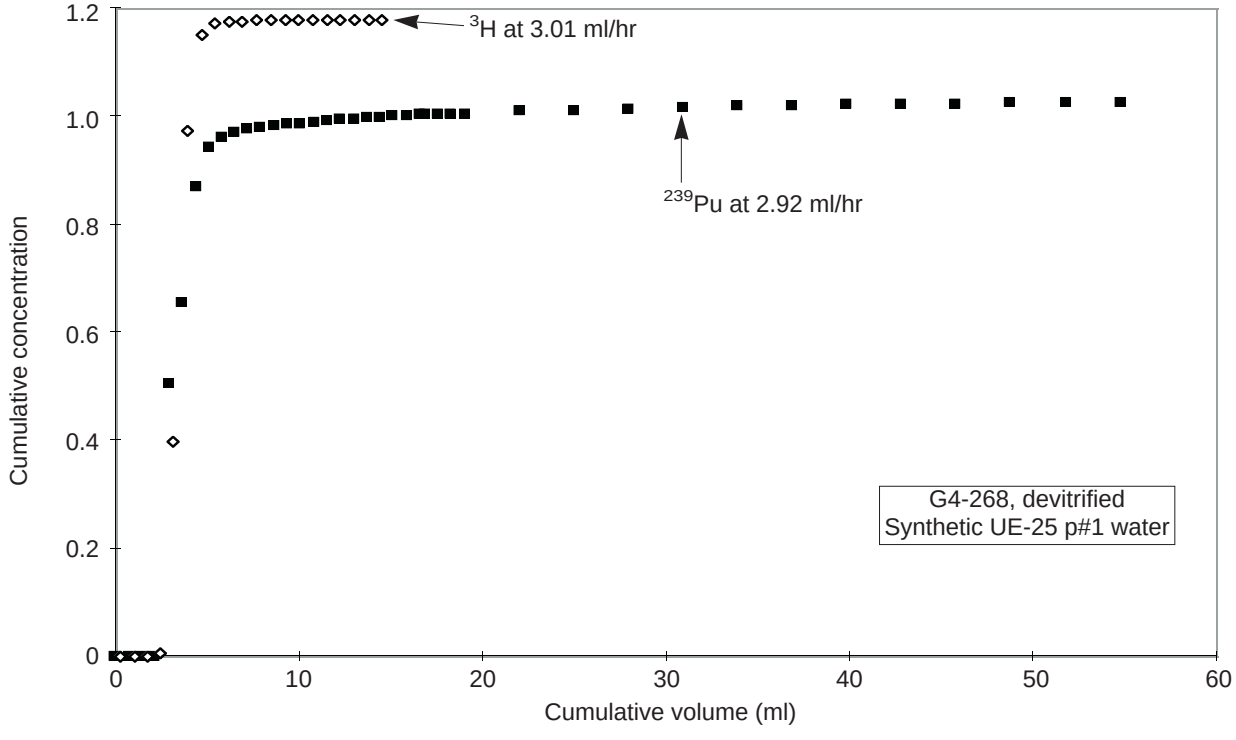

Figure 100. Column 3: Plutonium through Devitrified Tuff. This plot shows the elution curves for tritium and plutonium-239 through devitrified tuff sample G4-268 with synthetic UE-25 p#1 water.

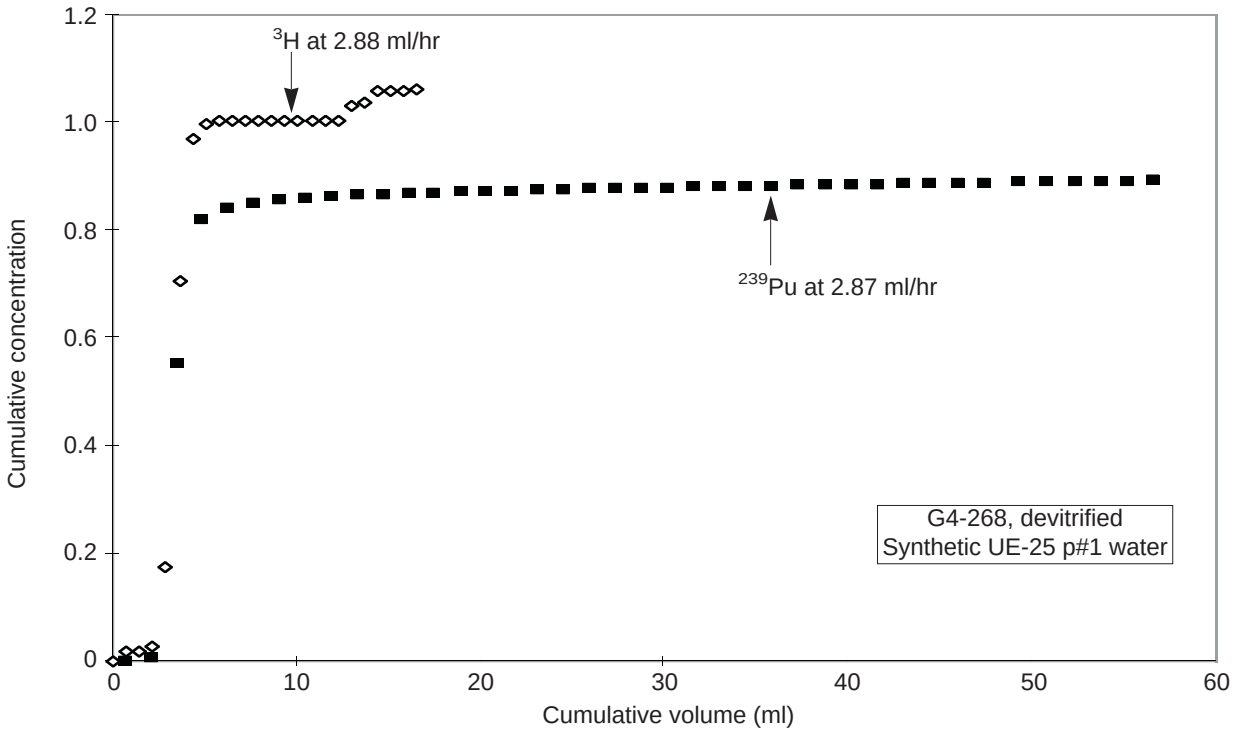

Figure 101. Column 4: Plutonium through Devitrified Tuff. This plot shows a second set of elution curves for tritium and plutonium-239 through devitrified tuff G4-268 with synthetic UE-25 p#1 water.

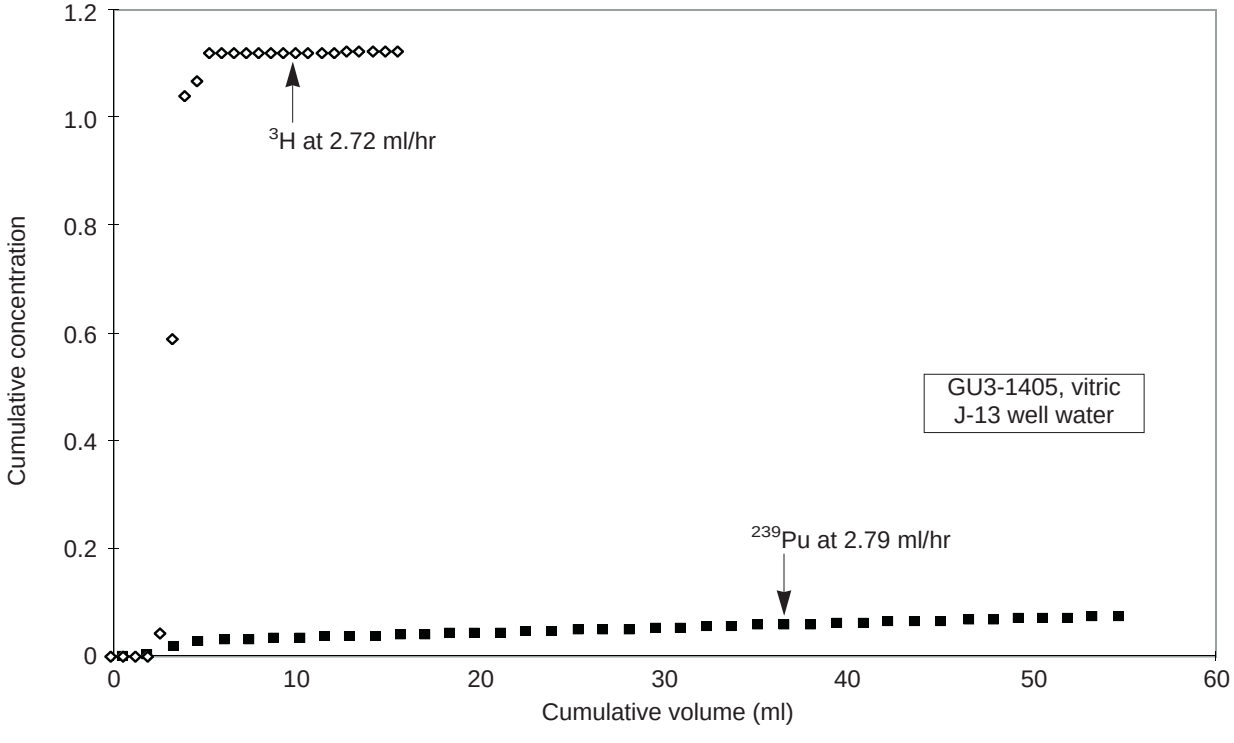

Figure 102. Column 5: Plutonium through Vitric Tuff. This plot shows the elution curves for tritium and plutonium-239 through vitric tuff sample GU3-1405 with J-13 well water.

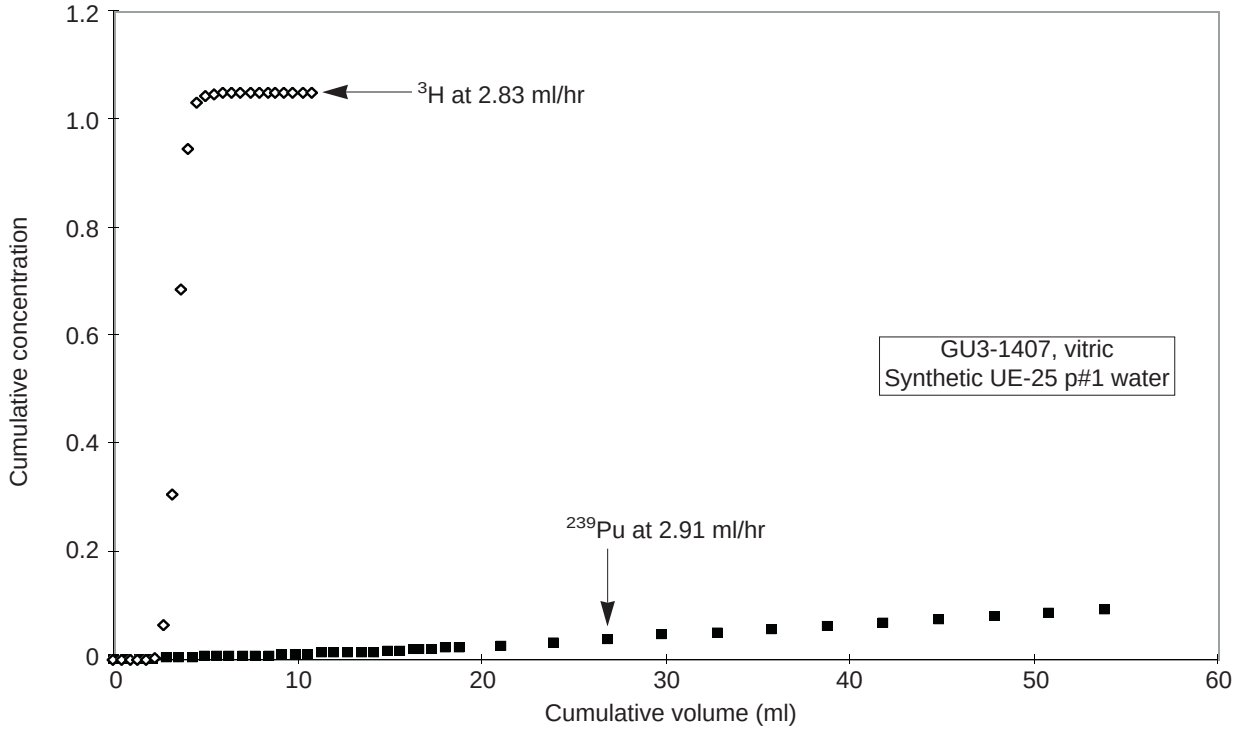

Figure 103. Column 6: Plutonium through Vitric Tuff. This plot shows the elution curves for tritium and plutonium-239 through vitric tuff sample GU3-1407 with synthetic UE-25 p#1 water.

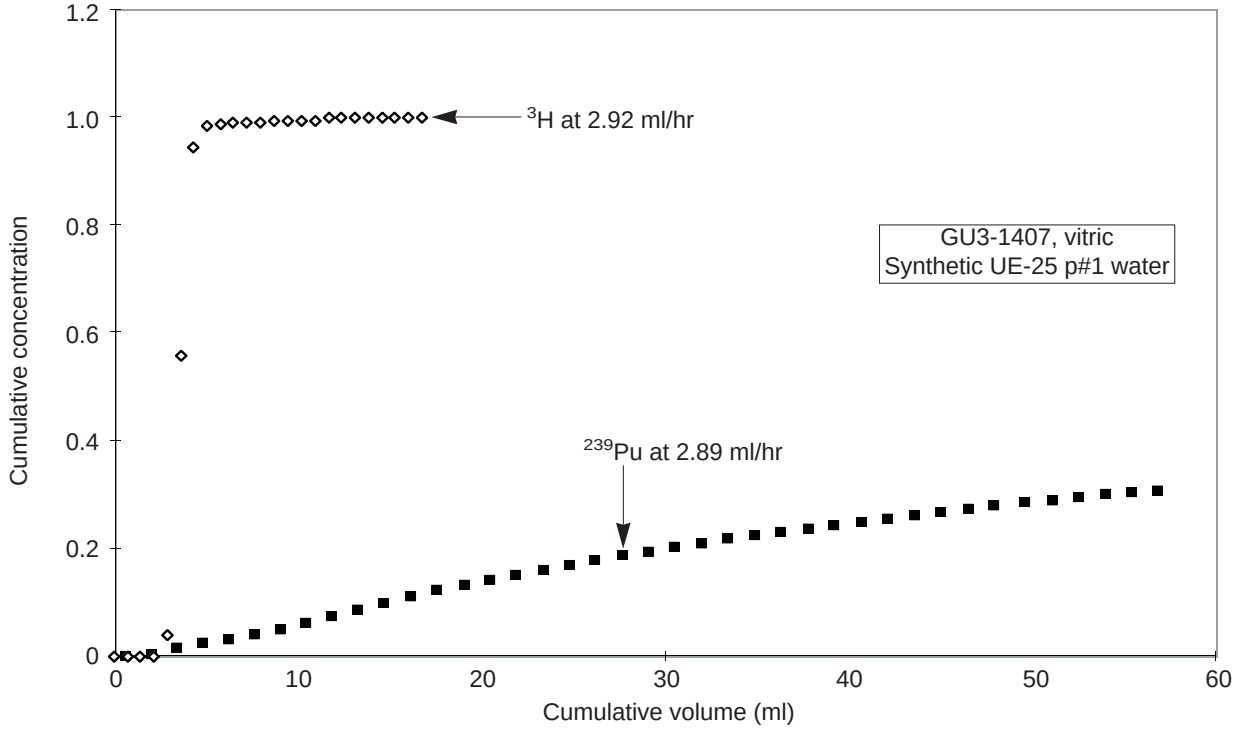

Figure 104. Column 7: Plutonium through Vitric Tuff. This plot shows another set of elution curves for tritium and plutonium-239 through vitric tuff sample GU3-1407 with synthetic UE-25 p#1 water.

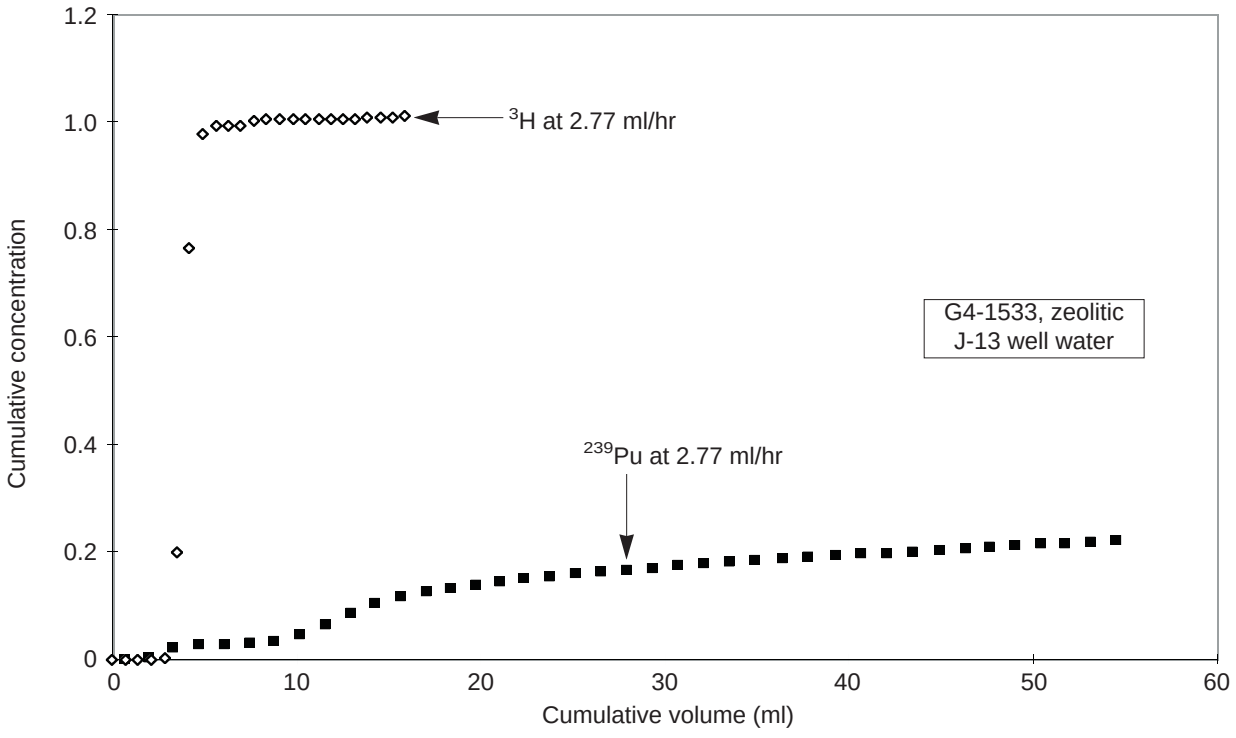

Figure 105. Column 8: Plutonium through Zeolitic Tuff. This plot shows the elution curves for tritium and plutonium-239 through zeolitic tuff sample G4-1533 with J-13 well water.

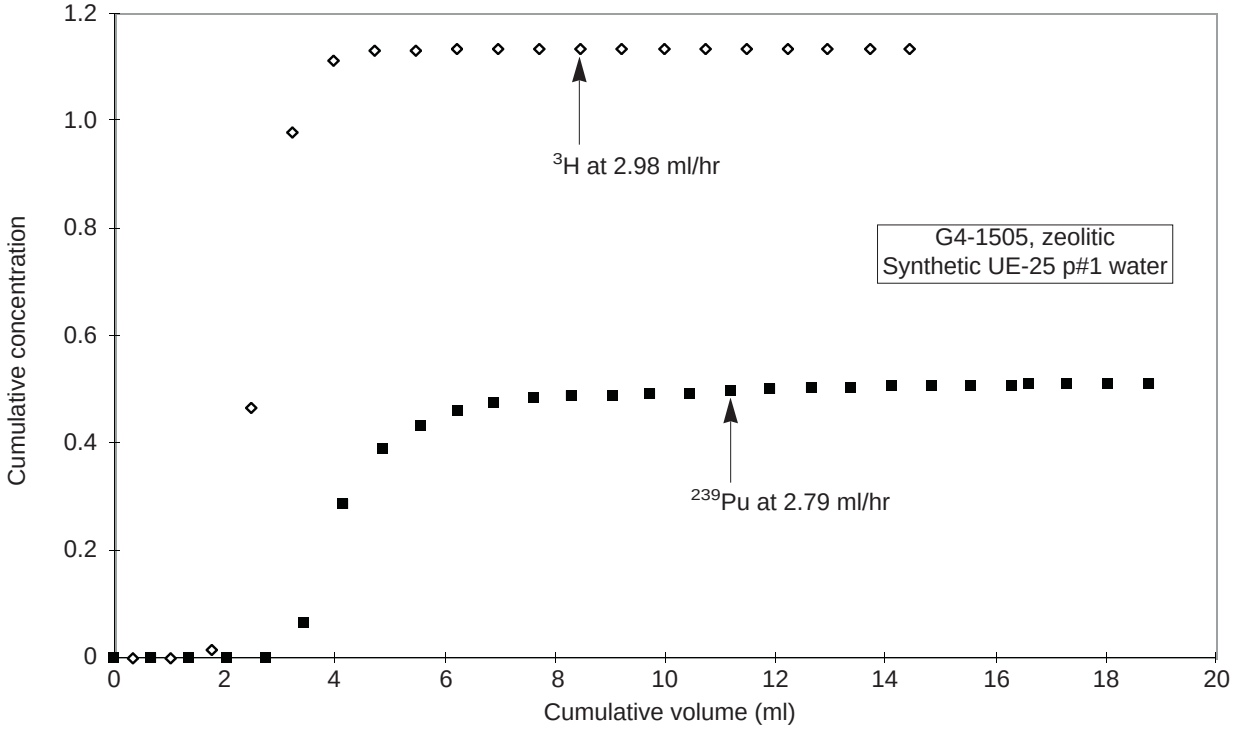

Figure 106. Column 9: Plutonium through Zeolitic Tuff. This plot shows the elution curves for tritium and plutonium-239 through zeolitic tuff sample G4-1505 with synthetic UE-25 p#1 water.

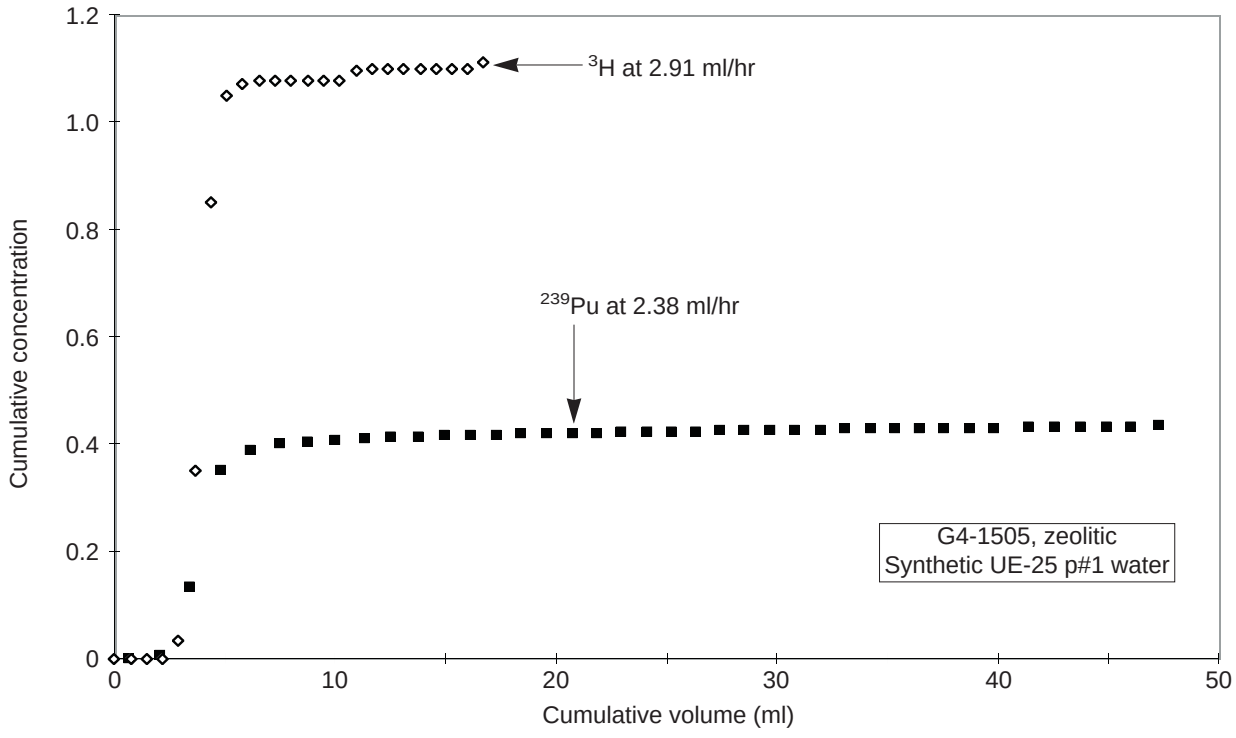

Figure 107. Column 10: Plutonium through Zeolitic Tuff. This plot shows the elution curves for tritium and plutonium-239 through zeolitic tuff sample G4-1505 with synthetic UE-25 p#1 water.

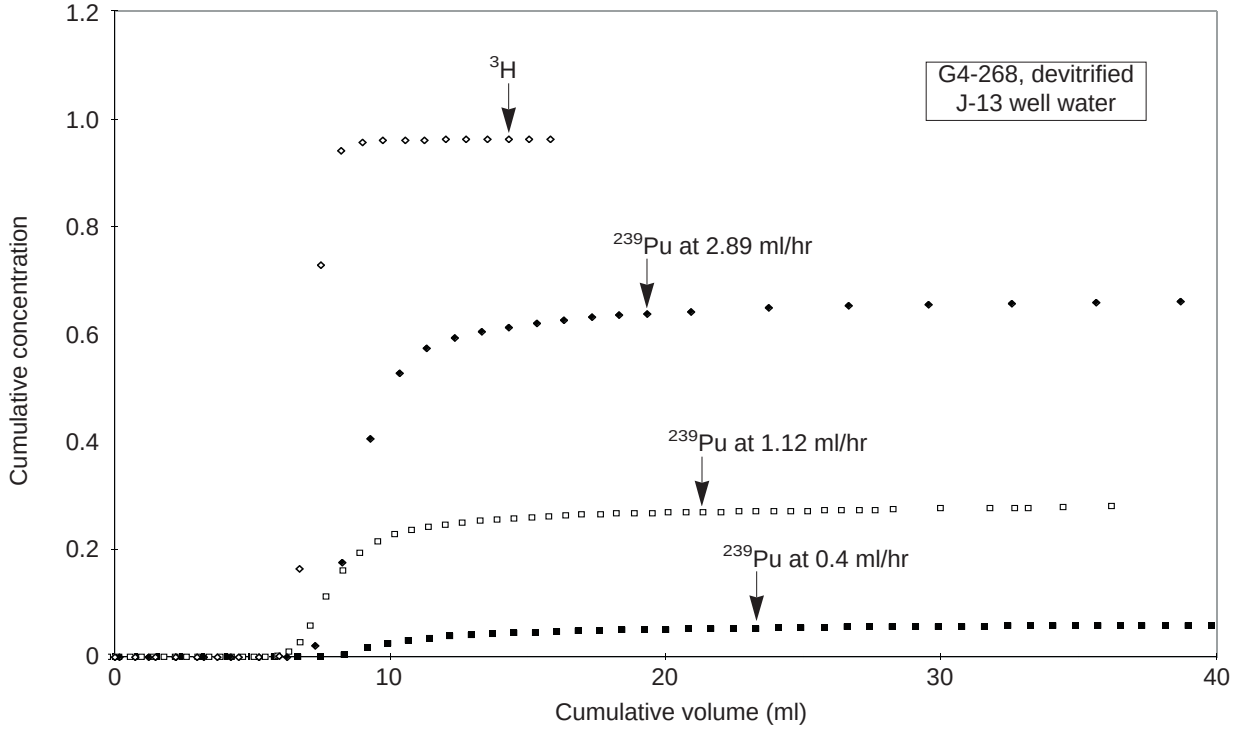

Figure 108. Column 11: Plutonium in Devitrified Tuff at Various Flow Rates. This plot shows elution curves for tritium and plutonium-239 at different flow rates with J-13 water through devitrified tuff G4-268.

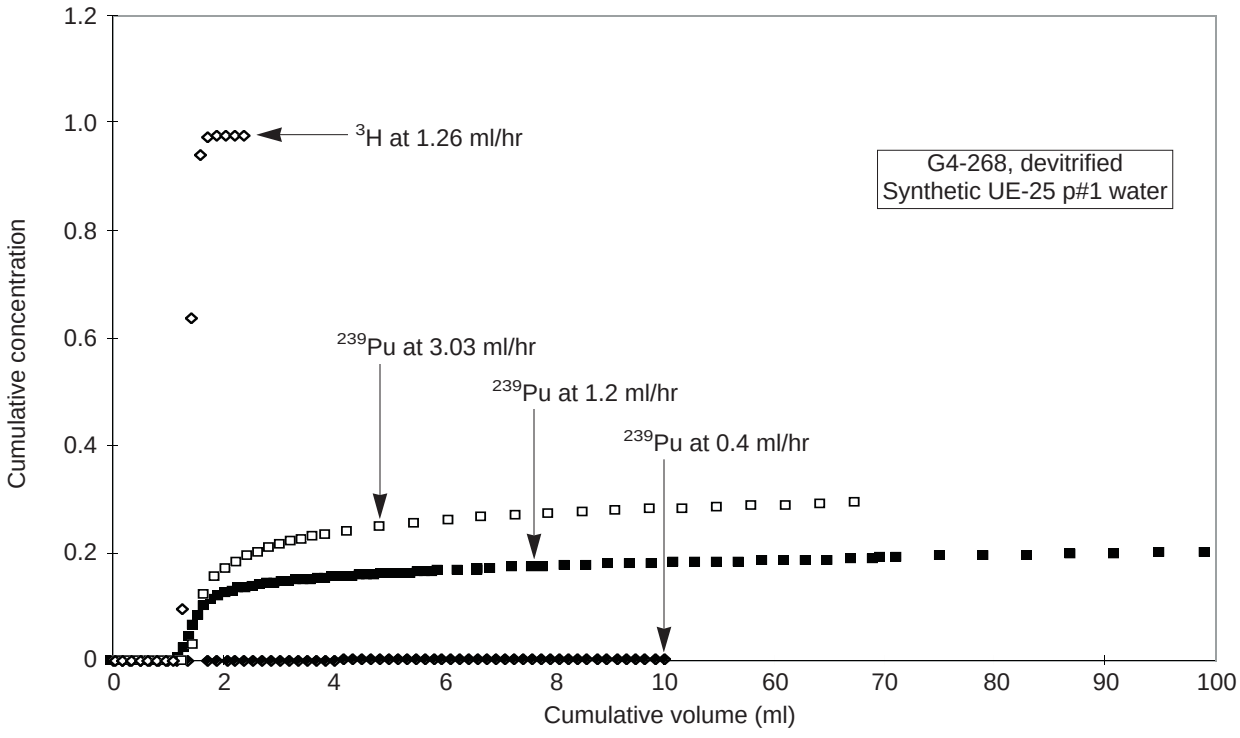

Figure 109. Column 12: Plutonium in Devitrified Tuff at Various Flow Rates. This plot shows elution curves for tritium and plutonium-239 at different flow rates in synthetic UE-25 p#1 water and tuff G4-268.

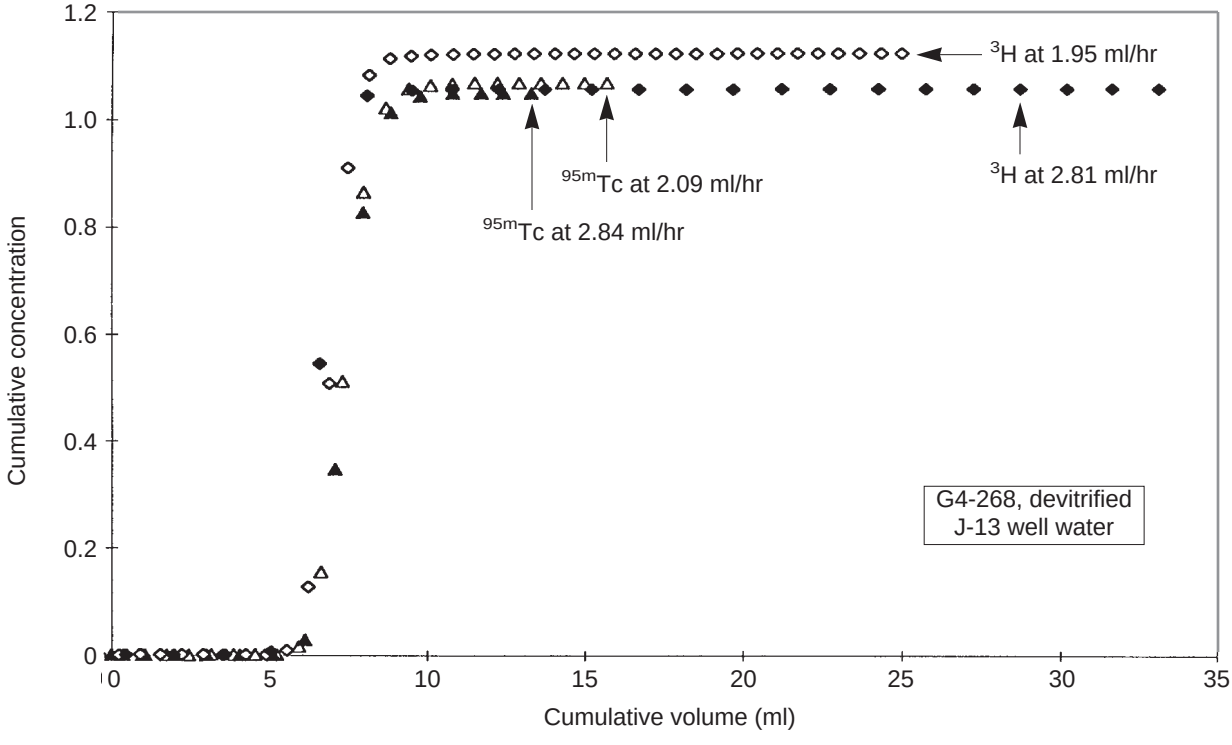

Figure 110. Column 13: Technetium in Devitrified Tuff. This plot shows the elution curves for tritium and technetium-95m at different flow rates with J-13 well water through devitrified tuff sample G4-268.

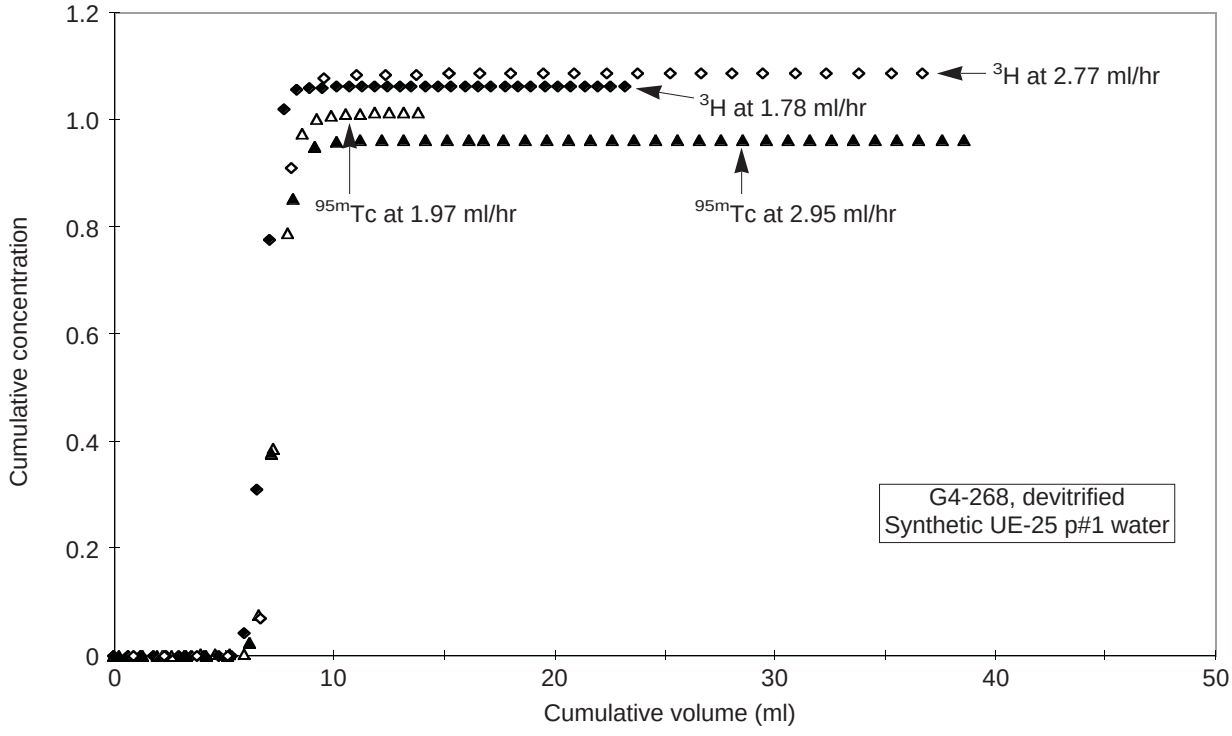

Figure 111. Column 14: Technetium in Devitrified Tuff. This plot shows the elution curves for tritium and technetium-95m at different flow rates with synthetic UE-25 p#1 water through devitrified tuff G4-268.

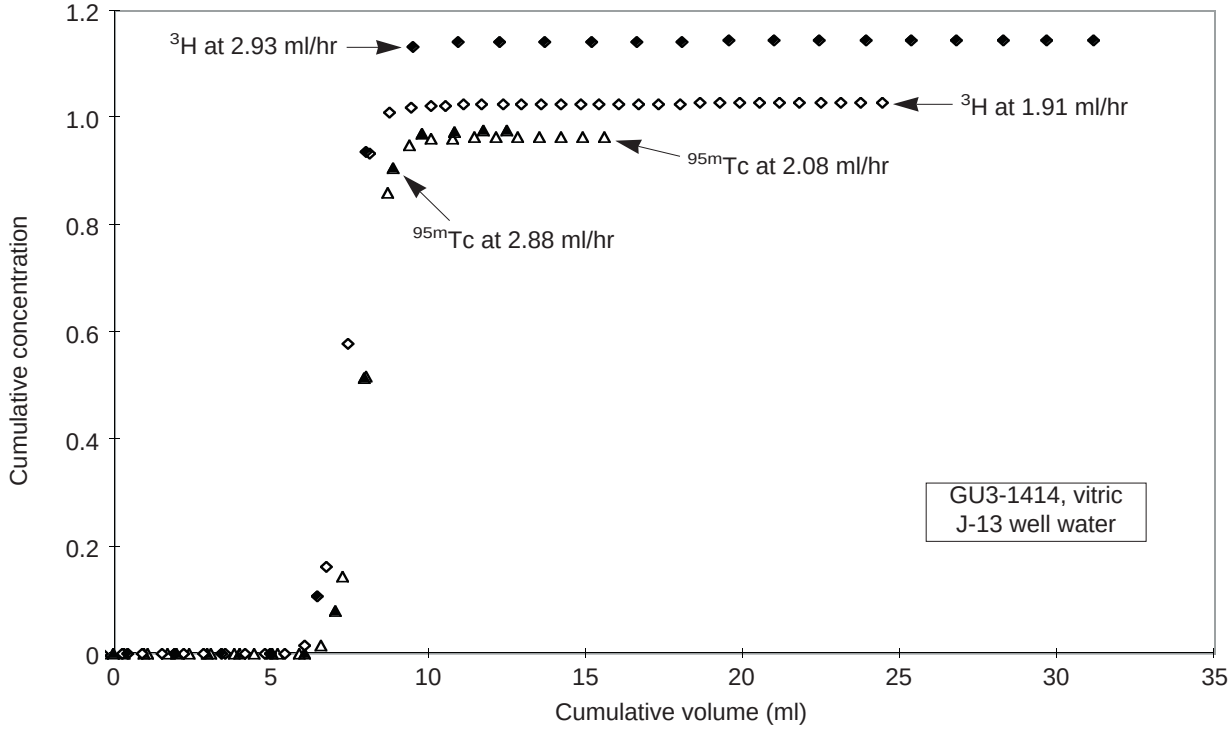

Figure 112. Column 15: Technetium in Vitric Tuff. This plot shows the elution curves for tritium and technetium-95m at different flow rates with J-13 well water through vitric tuff sample GU3-1414.

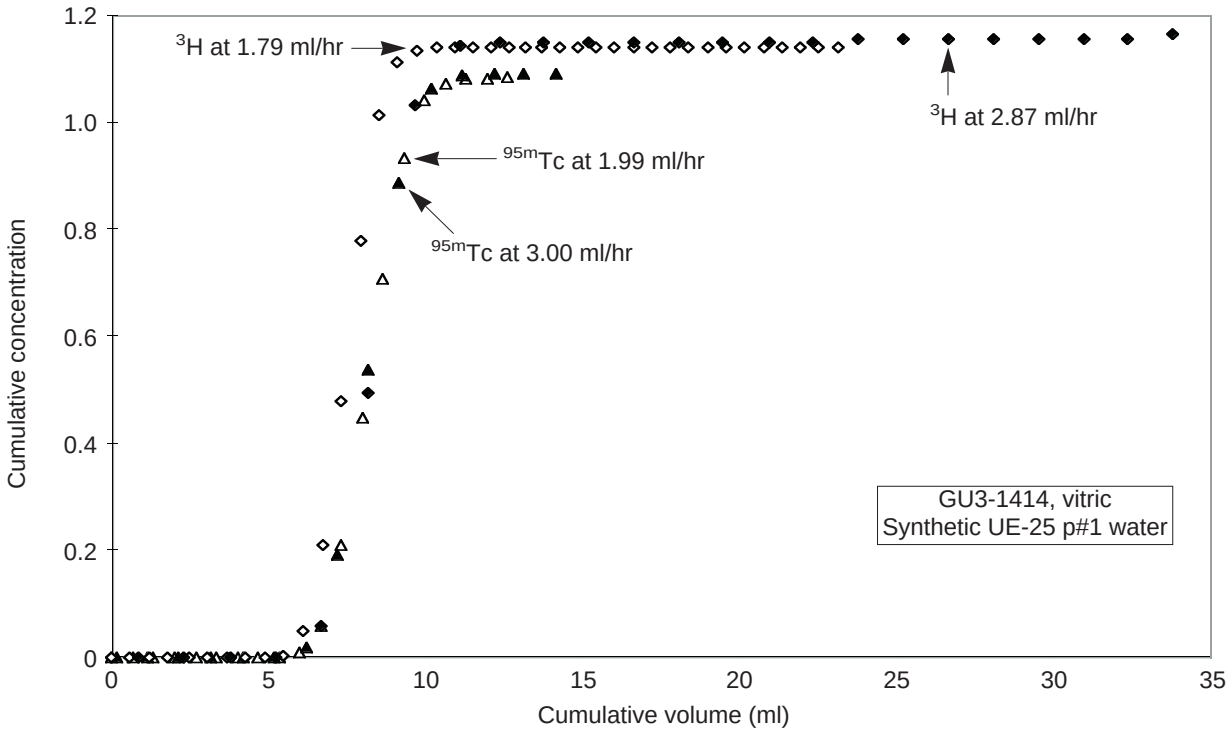

Figure 113. Column 16: Technetium in Vitric Tuff. This plot shows the elution curves for tritium and technetium-95m at different flow rates with synthetic UE-25 p#1 water through vitric tuff GU3-1414.

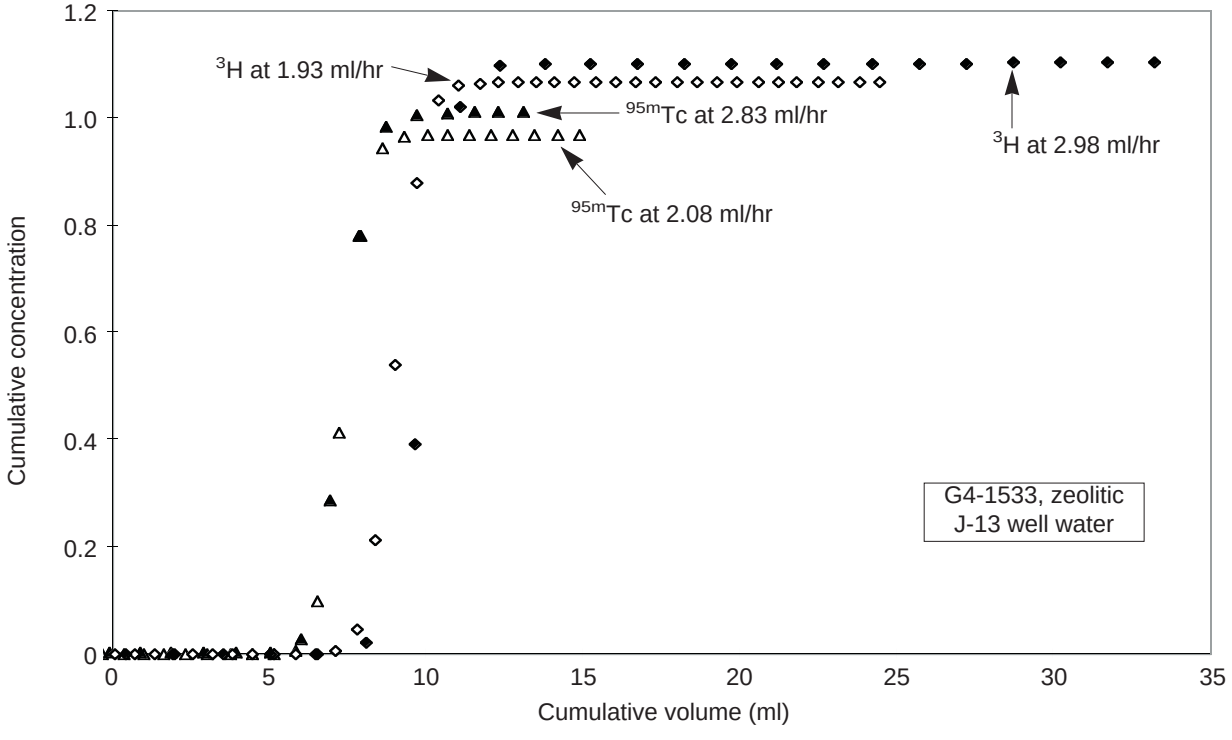

Figure 114. Column 17: Technetium in Zeolitic Tuff. This plot shows the elution curves for tritium and technetium-95m at different flow rates with J-13 well water through zeolitic tuff sample G4-1533.

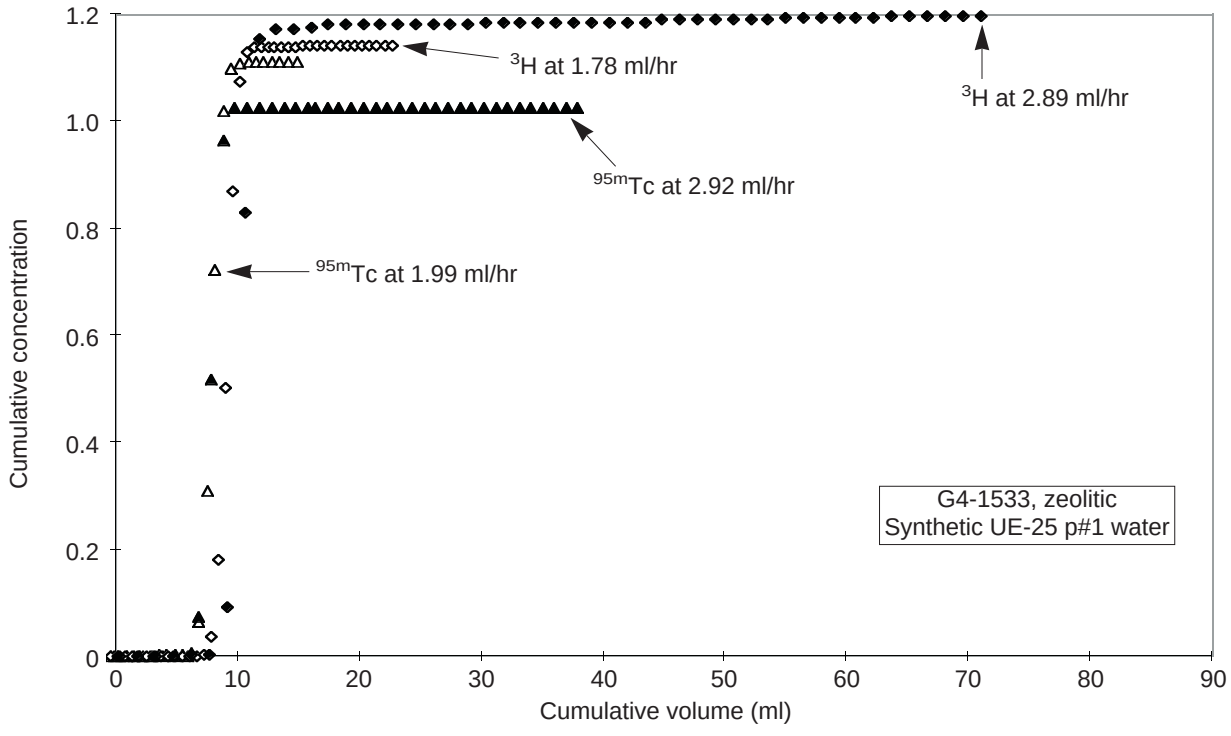

Figure 115. Column 18: Technetium in Zeolitic Tuff. This plot shows the elution curves for tritium and technetium-95m at different flow rates with synthetic UE-25 p#1 water through zeolitic tuff G4-1533.